NASA Contractor Report 191025

Laser-Saturated Fluorescence Measurements in Laminar Sooting Diffusion Flames

Changlie Wey
Sverdrup Technology, Inc.
Lewis Research Center Group
Brook Park, Ohio

May 1993

Prepared for
Lewis Research Center
Under Contract NAS3-24105

National Aeronautics and
Space Administration

LASER-SATURATED FLUORESCENCE MEASUREMENTS IN LAMINAR SOOTING DIFFUSION FLAMES

Changlie Wey
Sverdrup Technology, Inc.
Lewis Research Center Group
Brook Park, Ohio 44142

SUMMARY

The hydroxyl radical is known to be one of the most important intermediate species in the combustion processes. The hydroxyl radical has also been considered a dominant oxidizer of soot particles in flames. In this investigation the hydroxyl concentration profiles in sooting diffusion flames were measured by the laser-saturated fluorescence (LSF) method. The temperature distributions in the flames were measured by the two-line LSF technique and by thermocouple. In the sooting region the OH fluorescence was too weak to make accurate temperature measurements. The hydroxyl fluorescence profiles for all four flames presented herein show that the OH fluorescence intensities peaked near the flame front. The OH fluorescence intensity dropped sharply toward the dark region of the flame and continued declining to the sooting region. The OH fluorescence profiles also indicate that the OH fluorescence decreased with increasing height in the flames for all flames investigated. Varying the oxidizer composition resulted in a corresponding variation in the maximum OH concentration and the flame temperature. Furthermore, it appears that the maximum OH concentration for each flame increased with increasing flame temperature.

INTRODUCTION

The hydroxyl radical is known to be one of the most important intermediate species in the combustion process. The hydroxyl radical has also been considered a dominant oxidizer of soot particles in flames (Fenimore and Jones, 1967; Neoh et al., 1981). Because of its importance the hydroxyl radical has been studied extensively in a wide variety of experiments including shock tubes, photolysis, and flames. Laser-induced fluorescence (LIF) and laser-saturated fluorescence (LSF) techniques have been developed to measure the hydroxyl radical concentration in flames. The saturated fluorescence method has several advantages over the linear fluorescence method: The fluorescence signal is insensitive to both collisional quenching and laser power fluctuations, and the fluorescence signal is maximized for complete saturation.

Since LSF was proposed by Piepmeier (1972) and Daily (1977) as a combustion diagnostics tool, it has been used to measure the flame radicals CH (Bonczyk and Shirley, 1979), C_2 (Baronavski and McDonald, 1977), NH (Salmon et al., 1984), and OH (Lucht et al., 1983; Carter et al., 1987; Kohse-Höinghaus et al., 1984) in both atmospheric and low-pressure flames, but surprisingly almost all of this work has been carried out in nonsooting premixed flames. Some of those experiments showed discrepancies of factors of two to five when the fluorescence measurements were compared with the absorption measurements. These large errors are partly due to oversimplified assumptions and partly due to only partial saturation. Later, however, Lucht et al. (1985) developed the so-called balanced-cross-rate model, which states that the population in the laser-coupled levels remains approximately constant and equal to the initial population of the lower level because the rates of transfer into and out of the coupled level are balanced. Lucht et al. used this model to obtain better results. The objective of this study was to use the LSF technique to measure the hydroxyl (OH) concentration profile and temperature distribution in sooting diffusion flames at atmospheric pressure.

LASER FLUORESCENCE METHODS

In laser-induced fluorescence the molecules initially in a rotational energy level within the lower vibrational level v'' of the ground electronic state ($X^2\Pi$ for OH) are excited through photon absorption to a rotational level in the ground vibrational level v' of the first upper electronic state ($A^2\Sigma^+$ for OH). In the two-level molecular model once the molecule is in an excited state it can decay back to the ground state either through spontaneous emission or collisional energy-transfer (collisional quenching) processes (fig. 1). The rate and conservation equation for populations of the upper laser-coupled level is (Eckbreth, 1988; Lucht et al., 1985)

$$\frac{dN_2}{dt} = N_1 B_{12} I_{12} - N_2(B_{21} I_{12} + A_{21} + Q_{21}) \tag{1}$$

where

N_1 number density of lower laser-coupled level, cm^{-3}
N_2 number density of upper laser-coupled level, cm^{-3}
I_{12} laser spectral energy density, erg-sec/cm^3
B_{12} Einstein coefficient for absorption, cm^3/erg-sec^2
B_{21} Einstein coefficient for stimulated emission, cm^3/erg-sec^2
A_{21} spontaneous emission rate constant, sec^{-1}
Q_{21} collisional quenching rate constant, sec^{-1}

The population of the laser-coupled levels can be related to the unperturbed population N^o of the lower laser-coupled level by

$$N^o = N_1 + N_2 \tag{2}$$

Upon laser excitation the population peaks and the steady-state conditions apply, so that equation (1) becomes

$$N_2 = N^o \frac{B_{12}}{B_{21} + B_{12}} \left[1 + \frac{Q_{21} + A_{21}}{(B_{12} + B_{21}) I_{12}} \right]^{-1} \tag{3}$$

The observed fluorescence signal S_{FL} will be

$$S_{FL} = N_2 A_{21} \nu_{21} C_{\text{ref}} \tag{4}$$

where ν_{21} (cm^{-1}) is the transition frequency and C_{ref} is the calibration constant based on measurement at a reference condition.

If the laser excitation is at the unsaturated limit (i.e., $(B_{12} + B_{21})I_{12} << (Q_{21} + A_{21})$), equation (3) becomes

$$N_2 = N^o \frac{B_{12} I_{12}}{Q_{21} + A_{21}} \tag{5}$$

Hence in the linear fluorescence region

$$S_{FL} = N^o B_{12} I_{12} \frac{A_{21}}{Q_{21} + A_{21}} \nu_{21} C_{\text{ref}} \tag{6}$$

The fluorescence signal is related to the desired number density N^o, the laser power, and the collisional quenching rate constant Q_{21}. If the characteristic lifetime of the excited state $(A_{21} + Q_{21})^{-1}$ is longer than the laser pulse falltime and the signal detection system can temporally resolve the fluorescence signal, the quenching rate might be measured directly. However, variations in the collisional quenching rates, such as gas density, temperature, and composition change through the flame, and fluctuations in laser power cause difficulties in determining concentrations in the linear fluorescence region.

In the saturated laser power region (i.e., $(B_{12} + B_{21})I_{12} >> (Q_{21} + A_{21})$) equation (3) becomes

$$N_2 = N_{2S} = N^o \frac{B_{12}}{B_{21} + B_{12}} = N^o \frac{g_2}{g_1 + g_2} \tag{7}$$

where g_1 and g_2 are the respective degeneracies of the upper and lower laser-coupled levels and $g_1 B_{12} = g_2 B_{21}$. The fully saturated fluorescence signal is now only proportional to the desired number density and is independent of both the laser power and the quenching rate. Equation (3) can be rewritten as

$$N_2 = N_{2S}\left[1 + \frac{Q_{21} + A_{21}}{(B_{12} + B_{21})I_{12}}\right]^{-1} = N_{2S} W_{\text{sat}} = N^o \left(\frac{g_2}{g_1 + g_2}\right) W_{\text{sat}} \tag{8}$$

where W_{sat} is the degree of saturation. By combining equations (4) and (7), the saturated fluorescence signal becomes

$$S_{FL} = N^o \frac{g_2}{g_1 + g_2} A_{21} \nu_{21} C_{\text{ref}} W_{\text{sat}} \tag{9}$$

and

$$N^o = \left(\frac{g_1 + g_2}{g_2}\right) \frac{S_{FL}}{A_{21} \nu_{21} C_{\text{ref}} W_{\text{sat}}} \tag{10}$$

The total species number density N_T is related to N^o through the Boltzmann fraction F_t as

$$N_T = \frac{N^o}{F_t} \tag{11}$$

and

$$F_t = \frac{g_1}{Q} \exp\left(-\frac{hcE_1}{kT_f}\right) \tag{12}$$

where h is Planck's constant, c is the speed of light in vacuum, k is Boltzmann's constant, E_1 (cm^{-1}) is the level energy, $Q(= Q_{vib}Q_{rot}Q_{el})$ is the total molecule partition function, and T_f is the flame temperature. To determine species concentration, local flame temperature must be measured or estimated. However, the lower laser-coupled level can be chosen such that F_t is a weak function of temperature in order to reduce the temperature effect on concentration determination.

EXPERIMENTAL APPARATUS

Wolfhard-Parker Burner

A two-dimensional Wolfhard-Parker slot diffusion flame burner was selected for this investigation because it produces a pair of vertical, flat flame sheets that spatially separate the flame pyrolysis zone from the soot nucleation zone. This burner can yield more accurate absorption measurements without the need for deconvolution techniques to obtain local extinction coefficients as is necessary for cylindrically symmetric flames. The burner consists of three parallel slots 50.8 mm in length. The outer slots, which carry the oxidizer, are each 22.2 mm wide; the inner (fuel) slot is 6.4 mm wide. The burner is surrounded by a nitrogen shroud to exclude room air drafts and to prevent end-flamelets from forming across the width of the fuel slot. Further flame stabilization is assured by the use of screens near the tips of the flame.

The fuel and oxidizer passages each contain a section filled with 2- to 3-mm-diameter Pyrex glass beads to provide a uniform exit flow profile. A Hastalloy honeycomb section is used as the final section of the fuel and oxidizer passages. The flow conditions chosen for these studies resulted in underventilated flames (Gaydon and Wolfhard, 1979).

The openings that permit the passage of the incident, transmitted, and scattered beams are placed at preselected positions in the outer shield. The scattering opening is covered by an optically flat, fused quartz window. Scattered light is collected over a fixed solid angle and passed through this optical glass to the detector system. The incident and transmitted openings are each covered by a high-energy laser window.

The burner is cooled by water to ensure a consistent flame over extended running periods without overheating the facility. The burner can be displaced in the vertical and horizontal directions to enable measurements to be carried out in different parts of the flame without disturbing the optical system. The movement of the burner is controlled by a Velmax 8300 controller that is programmed by a DEC PDP–11/23 computer.

Flame Conditions

The burner was operated at atmospheric pressure. Flow rates and flame conditions for several flames are listed in table I. The structure of the flame used in this investigation is similar to that described in the literature (Wolfhard and Parker, 1952; Haynes and Wagner, 1980; Wey et al., 1984). The diffusion flame consists of an oxidant side and a fuel side that are separated by a reaction zone. The flame stabilizes itself toward the oxidant side of the burner. Because one unit volume of fuel requires more than one unit volume of oxidant for complete combustion, the stoichiometric fuel-oxidant interface moves outward into the oxidant side. A thin band of blue emission locates the main reaction zone. The sooting zone occurs some millimeters to the fuel side of the reaction zone. it is characterized by its familiar yellow luminosity. Between the sooting zone and the reaction zone there is a thin dark region that may be attributed to the absence of suitable emitters (Gaydon and Wolfhard, 1979). The yellow luminous region first becomes visible at a height of 5 to 10 mm above the burner depending on the flow conditions.

Temperature Measurements

The temperature distribution of the flame in this study was measured by the two-line LSF and thermocouple methods. The two-line LSF temperature measurements were performed by exciting the $Q_1(7)$ and $Q_1(15)$ lines and measuring the fluorescence intensity of the $P_1(8)$ and $P_1(16)$ lines, respectively. The rotational temperature T_{rot} is calculated from the ratio of the fluorescence intensities from two different excitation-emission pairs. For most flame conditions the OH rotational temperature T_{rot} is equal to the flame temperature T_f.

Combining equations (8) and (10) yields a working equation

$$S_{FL} = \frac{N_T}{Q}\left(\frac{g_1 g_2}{g_1 + g_2} A_{21}\nu_{21}\right) C_{ref} W_{sat} \exp\left(-\frac{hcE_1}{kT_f}\right) \tag{13}$$

$$S_{FL} = \frac{N_T}{Q} C_f C_{ref} W_{sat} \exp\left(-\frac{hcE_1}{kT_f}\right)$$

$$C_f = \frac{g_1 g_2}{g_1 + g_2} A_{21}\nu_{21}$$

where the constant C_f for each line pair can be calculated from Boltzmann statistics. Writing equation (13) for two given initial levels m and n and solving the resulting equations give

$$R = \frac{S_{FL,m}}{S_{FL,n}} = \frac{C_{f,m} C_{ref,m}}{C_{f,n} C_{ref,n}} \exp\left[-\frac{hc(E_{1,m} - E_{1,n})}{kT_f}\right] \tag{14}$$

Let

$$\beta = \left(\frac{C_{f,n}}{C_{f,m}}\right)\left(\frac{C_{ref,n}}{C_{ref,m}}\right), \quad \Delta E_1 = E_{1,n} - E_{1,m} \tag{15}$$

Then

$$T_f = \frac{hc\,\Delta E_1}{k \ln(\beta R)} \tag{16}$$

The thermocouple measurements were made with 75-μm-diameter Pt/Pt-13%Rh (type R) thermocouples. The thermocouple readings were uncorrected for radiation heat loss and were processed by the PDP–11/23 computer.

Fluorescence Measurements

The optical layout for the fluorescence measurements is shown in figure 2. The second harmonic of a Quanta-Ray DCR–2A Nd:YAG laser (at 532 nm) was used to pump a PDL–1 dye laser, which included a transversely pumped preamplifier and a longitudinally pumped amplifier. The laser dye Sulforhodamine 640 (SR640), whose

peak output is at 604.5 nm, was used for this measurement. To achieve high-energy output at 620 nm, the dye laser used a mixture of SR640 and DCM dye, whose peak output is at 640 nm. The DCM was added to the SR640 in 50-ml increments while monitoring the laser energy with the PDL–1 grating set at 620 nm. This procedure was continued until the laser energy reached the peak. Applying this procedure to both oscillator and amplifier resulted in a dye laser energy of about 40 mJ/pulse at 620 nm, with an input energy of about 190 mJ/pulse at 532 nm. The dye laser output was frequency doubled by a wavelength extension system (WEX–1A). A Pellin-Broca prism was used to disperse the visible and ultraviolet (UV) laser beams. A small portion of visible laser was then picked off by a quartz beam splitter and directed to the fast photodiode (Scientech 301–020). The output of the photodiode was used to trigger the detection electronics system. A 7-nsec laser pulse with 4 mJ of energy at a wavelength of 310 nm was directed by an antireflection-coated, fused-silica mirror. The laser beam was then focused into the flame zone parallel to the burner slots by using a 500-mm-focal-length, high-energy, antireflection-coated UV lens, which gave an approximate focal diameter of 0.6 mm. The fluorescence was collected at right angles to the laser beam by a 50-mm-diameter, 200-mm-focal-length coated-quartz lens. The fluorescence image was rotated from the horizontal to the vertical plane by a beam-steering instrument. The vertical fluorescence image was then focused by a 50-mm-diameter, 300-mm-focal-length coated lens onto the entrance slit of a computer-controlled SPEX model 1720 0.75-m spectrometer. For all the LSF measurements the entrance and exit slit widths were set at 50 μm. The bandpass of the spectrometer was therefore less than 1 Å. The fluorescence intensity was detected by an EMI 9954QB photomultiplier tube with nonuniform dynode-voltage distribution to obtain a 1-nsec rise time. The photomultiplier signal was then processed by the Stanford Research System boxcar integrator. The boxcar system includes two gated integrators, two fast samplers, an analog processor, a gate scanner, and a computer interface module. A Scientech 365 power and energy meter with a surface absorbing head was used to measure the average laser pulse energy after the beam had passed through the flame. The photodiode signal was also processed by the boxcar integrator. The output of the boxcar integrator was then digitized and stored by a DEC PDP–11/23 computer through a 16-bit analog-to-digital converter to determine the fluorescence intensity.

RESULTS AND DISCUSSION

Saturation Measurements

The degree of saturation by the laser was determined by adding calibrated neutral density (ND) filters into the laser beam path and measuring the corresponding fluorescence voltages. The fluorescence signal was averaged by boxcar integration for 2 min at each condition. From the known ND filter values and the averaged fluorescence voltage, a saturation curve was generated. Figure 3 shows a typical saturation curve for a measured $C_3H_8/O_2/N_2$ flame. Complete saturation of the OH fluorescence was nearly achieved. Because of the high degree of saturation achieved, hydroxyl number densities were calculated from the fluorescence induced by the unattenuated UV laser beam. The difference between the theoretical complete saturated fluorescence signal and the measured fluorescence signal was less than the experimental uncertainty in these LSF fluorescence measurements.

Temperature Profiles and OH Number Density

The $Q_1(7)$ rotational line of the $A^2\Sigma^+ - X^2\Pi(0,0)$ band of the hydroxyl was excited by the laser pulse. The $Q_1(7)$ line was identified with laser fluorescence excitation spectra measured in a flame. The dye laser was scanned near the $Q_1(7)$ line and the fluorescence was detected at $P_1(8)$. In the fluorescence measurements the wavelength of the dye laser was positioned at the peak of the $Q_1(7)$ line by maximizing the fluorescence signal. The same procedure was applied to the second excited rotational line $Q_1(15)$ for temperature measurement. The LSF system was calibrated by Rayleigh scattering from gas molecules (Salmon and Laurendeau, 1985). Three gases (nitrogen, methane, and ethylene) were used as the calibration scatterers. The ratios of the scattering cross

sections for the three gases were measured and compared with the calculated values. Nitrogen gas was used for the reference because it has the smallest cross-sectional area (5.40×10^{-27} cm^2 at 310 nm) and is easily handled. The Einstein coefficients and fundamental data for the hydroxyl radical were found from Goldman and Gillis (1981) and Dieke and Crosswhite (1962).

The gas temperature in the flames was determined both by the two-line LSF method and by a thermocouple. The temperature near the flame front measured by the two-line LSF was about 100 K below the calculated adiabatic flame temperature. In the sooting flame region the OH fluorescence signal was too weak to measure accurately. The two-line LSF temperature measurement, however, was limited by the difficulty of spatial alignment for our current single-laser system. When the dye laser grating was tuned to the second excitation line, the position of the focused UV beam spot was always different from that of the first excitation line. The optical alignment and calibration for the second excitation line also had to be carried out. Several iris diaphragms were placed in the laser beam path before and after the burner optical entry and exit ports to help in optical alignment. The UV laser beam was directed through the center of each iris diaphragm to ensure that the laser beam passed through the burner center. An argon ion laser was used to help align the UV beam focal point. The green laser beam was directed from the burner opposite port and focused at the burner center by a lens. Both the UV beam and the green laser beam were coincident at the burner center. The same procedure was applied when the excitation laser line was tuned to the second wavelength. However, the two UV-focused points, which were formed at two different times, were not completely coincident even with the alignment laser. Because the displacements of these two UV-focused points are three-dimensional and in the submillimeter range, they need to be determined by a precise instrument. The two-line LSF will be a versatile technique for measuring temperature distribution in flames if two dye lasers are simultaneously used and a precision optical alignment instrument is available.

In this study the OH fluorescence profiles were measured by exciting the $Q_1(7)$ and $Q_1(15)$ lines and measuring the fluorescence intensity of the $P_1(8)$ and $P_1(16)$ lines, respectively. Carefully comparing those two profiles shows that the temperature distribution can be calculated only near the flame front where the higher fluorescence readings were measured. Figure 4 shows the temperature profile near the flame front for flame A. The adiabatic flame temperature was calculated at the flame front, where the highest fluorescence reading occurred. The two-line LSF method has limitations in determining the temperature distribution in the flame as discussed earlier. However, the flame front temperature can be easily determined by this method from two peak fluorescence readings. Figure 5 shows the temperature profile measured by the thermocouple in flame B, which was the only flame temperature measured by the thermocouple. The temperatures in the flame front for flames A, C, and D were greater than the melting point of platinum (1755 °C), causing the thermocouple to break. The flame front temperatures of those flames were then determined by two-line LSF. Table II lists the comparison of measured flame temperature with calculated adiabatic temperature.

Figure 6 shows the OH fluorescence profile for flame A at different heights above the burner. The OH fluorescence peaked at the flame front and then decreased toward the sooting region. In the sooting region the soot scattering signal interfered with the fluorescence signal. In this region the fluorescence reading from 306 nm to 314 nm was much lower than that at the flame front. In the burner center the fluorescence was also low relative to the flame front. The fluorescence profile also shows that the local maximum fluorescence decreased with increasing height above the burner (fig. 7). Figure 8 shows the OH relative fluorescence profiles for flames B, C, and D, respectively. Each profile indicates the same trends: that the OH peaked at the flame front and that the maximum local value decreased with increasing height above the burner. The relative fluorescence profiles were converted to concentration measurements by using equation (10) with the calibration constant measured from the Rayleigh scattering in nitrogen. Figure 9 shows the concentration profiles for all investigated flames. Figure 10 shows the OH concentration profiles for all four flames measured at 5 mm above the burner. The concentration profiles were calculated up to the sooting region, where the error in temperature measurements by the two-line LSF method had a significant effect on the hydroxyl number density measurement.

In table II the measured hydroxyl concentrations and measured temperatures are compared with the calculated values. The adiabatic flame temperatures and hydroxyl mole fractions were calculated by using a NASA computer code (Gordon and McBride, 1971). The measured temperatures were all lower than the calculated values, and the measured hydroxyl concentrations were all higher than the calculated concentrations. However, the measured and calculated temperatures show the same trend; flame B had the lowest temperature. The concentration measurements also show the same trend. The concentration profiles show that the visible soot emission began after the OH concentration dropped sharply.

CONCLUSIONS

Some researchers have doubted that the hydroxyl radical is the dominant oxidizer of the soot particles in flames. In this investigation OH concentration profiles in sooting diffusion flames were measured by the laser-saturated fluorescence (LSF) method. The temperature distributions in the flames were measured by the two-line LSF technique and by a thermocouple. In the sooting region the OH fluorescence was too weak to measure accurately. The hydroxyl fluorescence profiles for all four flames presented here show that the OH fluorescence intensities peaked near the flame front. The OH fluorescence intensity dropped sharply toward the dark region of the flame and continued declining to the sooting region. The OH fluorescence profiles also indicate that the OH fluorescence decreased with increasing height in the flames for all flames investigated. Varying the oxidizer composition resulted in a corresponding variation in the maximum OH concentration and flame temperature. Furthermore, it appears that the maximum OH concentration for each flame increased with increasing flame temperature.

ACKNOWLEDGMENTS

This work was sponsored by the NASA Lewis Research Center under contract NAS3–24105, which was monitored by Dr. Edward J. Mularz.

REFERENCES

Baronavski, A.P., and McDonald, J.R., 1977, "Measurement of C_2 Concentrations in an Oxygen-Acetylene Flame: An Application of Saturation Spectroscopy," Journal of Chemical Physics, vol. 66, pp. 3300–3301.

Bonczyk, P.A., and Shirley, J.A., 1979, "Measurement of CH and CN Concentration in Flames by Laser-Induced Saturated Fluorescence, Combustion and Flame," vol. 34, pp. 253–264.

Carter, C.D., et al., 1987, "Feasibility of Hydroxyl Concentration Measurements by Laser Saturated Fluorescence in High Pressure Flames," Applied Optics, vol. 26, pp. 4551–4561.

Daily, J.W., 1977, "Saturation Effects in Laser Induced Fluorescence Spectroscopy," Applied Optics, vol. 16, pp. 568–571.

Dieke, G.H., and Crosswhite, H.M., 1962, "The Ultraviolet Bands of OH," Journal of Quantitative Spectroscopy and Radiative Transfer, vol. 2, pp. 97–199.

Eckbreth, A.C., 1988, Laser Diagnostics for Combustion Temperature and Species, Abacus Press, Cambridge, MA.

Fenimore, C.P., and Jones, C.W., 1967, "Oxidation of Soot by Hydroxyl Radicals," Journal of Physical Chemistry, vol. 71, pp. 593–597.

Gaydon, A.G., and Wolfhard, H.G., 1979, Flames: Their Structure, Radiation and Temperature, Fourth Edition, Chapman and Hall, London.

Goldman, A., and Gillis, J.R., 1981, "Spectral Line Parameters for the $A^2\Sigma - X^2\Pi(0,0)$ Band of OH for Atmospheric and High Temperatures," Journal of Quantitative and Radiative Transfer, vol. 25, pp. 111–135.

Gordon, S., and McBride, B.J., 1971, "Computer Program for Calculation of Complex Chemical Equilibrium Compositions, Rocket Performance, Incident and Reflected Shocks, and Chapman-Jouguet Detonations," NASA SP–273.

Haynes, B.S., and Wagner, H.G., 1980, "Sooting Structure in a Laminar Diffusion Flame," Berichte der Bunsen-Gesellschaft fuer Physikalische Chemie, vol. 84, pp. 499–506.

Kohse-Höinghaus, K., Perc, W., and Just, Th., 1984, "Determination of Absolute OH and CH Concentrations in a Low Pressure Flame by Laser-Induced Saturated Fluorescence," Nineteenth Symposium (International) on Combustion, The Combustion Institute, Pittsburgh, PA, pp. 1177–1185.

Lucht, R.P., Sweeney, D.W., and Laurendeau, N.M., 1983, "Laser Saturated Fluorescence Measurements of OH Concentration in Flames," Combustion and Flame, vol. 50, pp. 189–205.

Lucht, R.P., Sweeney, D.W., and Laurendeau, N.M., 1985, "Laser Saturated Fluorescence Measurements of OH in Atmospheric Pressure $CH_4/O_2/N_2$ Flames Under Sooting and Nonsooting Conditions," Combustion Science and Technology, vol. 42, pp. 259–281.

Neoh, K.G., Howard, J.B., and Sarofim, A.F., 1981, "Soot Oxidation in Flames," Particulate Carbon—Formation During Combustion, D.C. Seigla and G.W. Smith, eds., Plenum Press, New York, pp. 261–282.

Piepmeier, E.H., 1972, "Theory of Laser Saturated Atomic Resonance Fluorescence," Spectrochimica Acta, vol. 27B, pp. 431–443.

Salmon, J.T., et al., 1984, "Laser Saturated Fluorescence Measurements of NH in a Premixed Subatmospheric $CH_4/N_2O/Ar$ Flame," Twentieth Symposium (International) on Combustion, The Combustion Institute, Pittsburgh, PA, pp. 1187–1193.

Salmon, J.T., and Laurendeau, N.M., 1985, "Calibration of Laser Saturated Fluorescence Measurements Using Rayleigh Scattering," Applied Optics, vol. 24, pp. 65–73.

Wey, C., Powell, E.A., and Jagoda, J.I., 1984, "The Effect on Soot Formation of Oxygen in the Fuel of a Diffusion Flame," Twentieth Symposium (International) on Combustion, The Combustion Institute, Pittsburgh, PA, pp. 1017–1024.

Wolfhard, H.G., and Parker, W.G., 1952, "A Spectroscopic Investigation of the Structure of Diffusion Flame," Proceedings of the Physical Society, Sec. A, vol. 65, pp. 2–19.

TABLE I.—FLOW CONDITIONS FOR ATMOSPHERIC PRESSURE DIFFUSION FLAMES ON A 5.08-cm-LONG THREE-SLOT WOLFHARD-PARKER BURNER

[Fuel, propane at 580 ml/min (3.0 cm/sec); oxidizer, total at 8120 ml/min (6.0 cm/sec); oxygen index, OI = oxygen/total oxidizer.]

Flame	Oxidizer	OI	Equilibrium mole fraction						
			H_2	H_2O	O_2	CO	CO_2	N_2	Ar
A	$O_2 + N_2$	0.28	0.009	0.18	0.016	0.035	0.112	0.627	------
B	$O_2 + CO_2$	.28	.001	.196	.012	.025	.763	------	------
C	O_2 + Ar	.28	.015	.163	.028	.055	.089	------	0.616
D	$O_2 + N_2$	.31	.012	.191	.02	.045	.114	.588	------

TABLE II.—COMPARISON OF HYDROXYL CONCENTRATION AND FLAME TEMPERATURE DATA FROM LASER-SATURATED FLUORESCENCE MEASUREMENTS WITH CALCULATED VALUES

[OH spectral line, $A^2\Sigma^+ - X^2\Pi(0,0)$; excitation, $Q_1(7)$ and $Q_1(15)$; observation, $P_1(8)$ and $P_1(16)$.]

Flame	Flame temperature, K		Hydroxyl number density, cm^{-3}		Mole fraction	
	Calculated	Measured	Calculated	Measured	Calculated	Measured
A	2512	[a]2405	3.15×10^{-16}	9.05×10^{-16}	0.01	0.03
B	2128	[b]1927	.89	3.49	.00	.01
C	2713	[a]2581	7.29	11.72	.03	.04
D	2584	[a]2515	4.17	9.58	.01	.03283

[a]Two-line LSF method.
[b]Thermocouple.

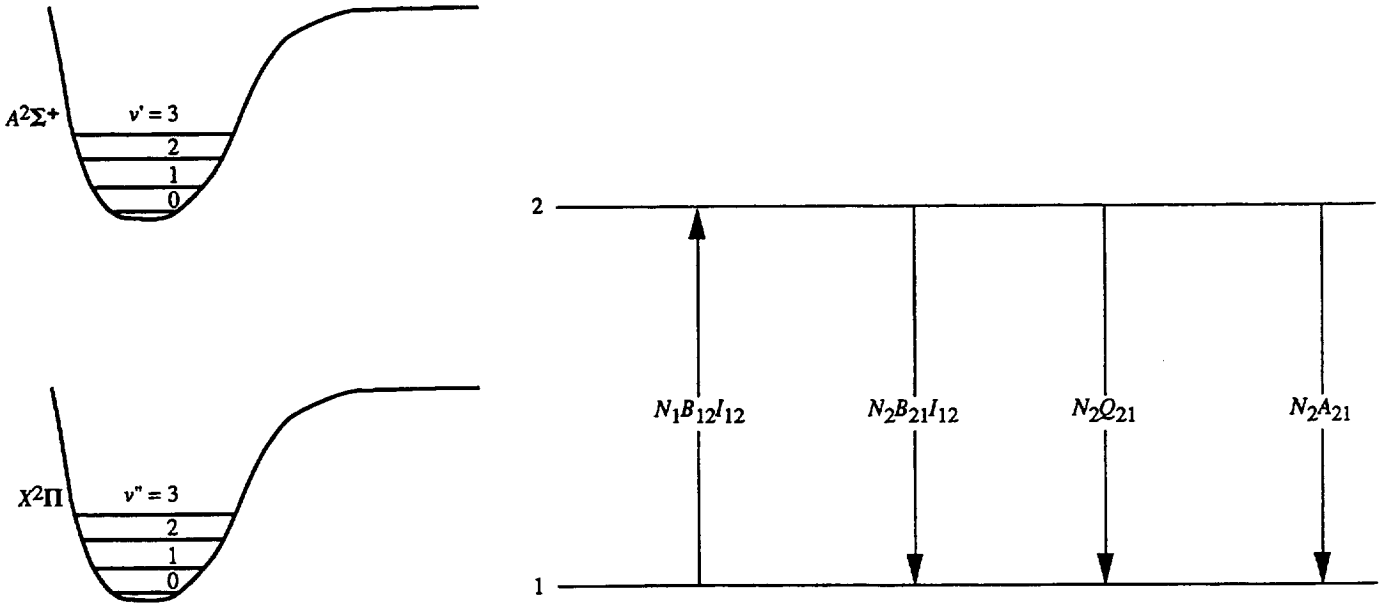

Figure 1.—OH energy level structure and population transfer scheme used in fluorescence measurements of hydroxyl concentration. B_{12} and B_{21} are the Einstein coefficients for absorption and stimulated emission, respectively. Q_{21} and A_{21} are the rate coefficients for collisional quenching and spontaneous emission, respectively.

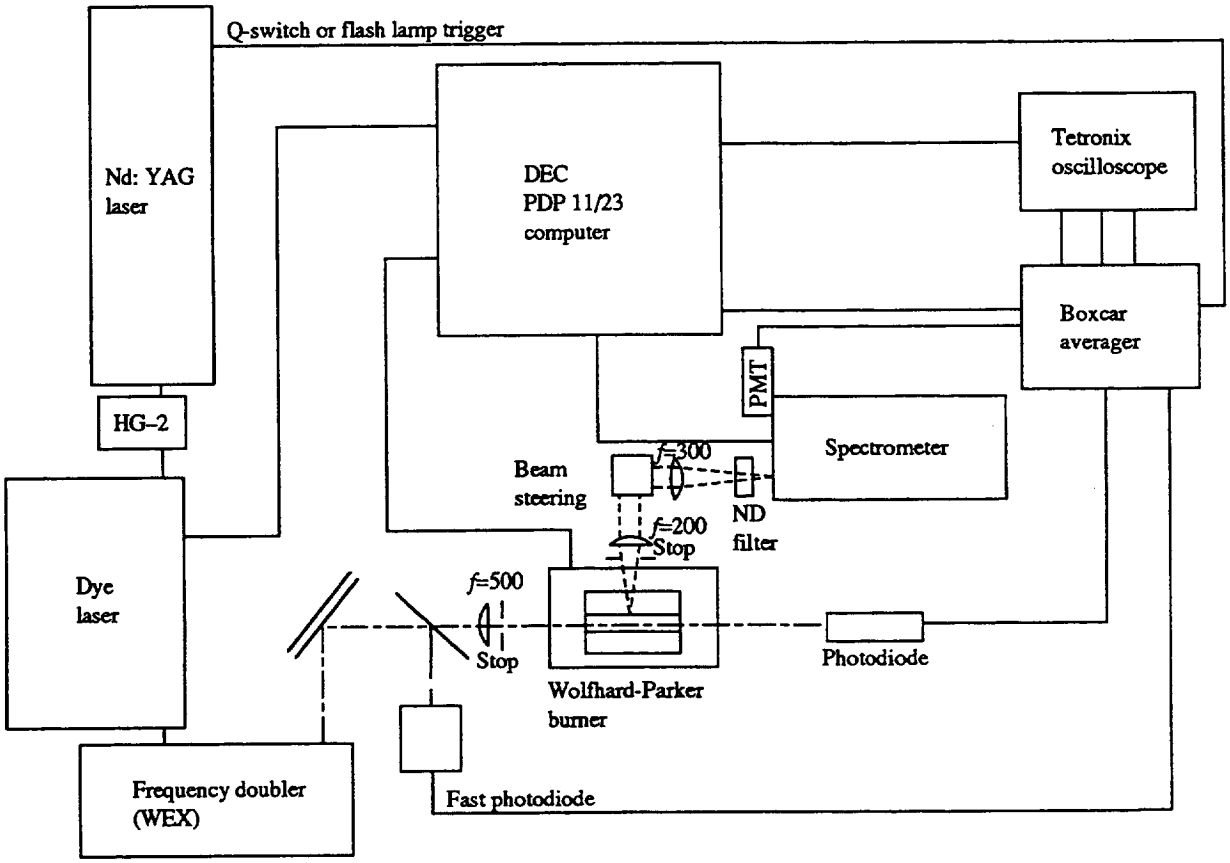

Figure 2.—Schematic of experimental setup and Wolfhard-Parker burner for LSF measurements.

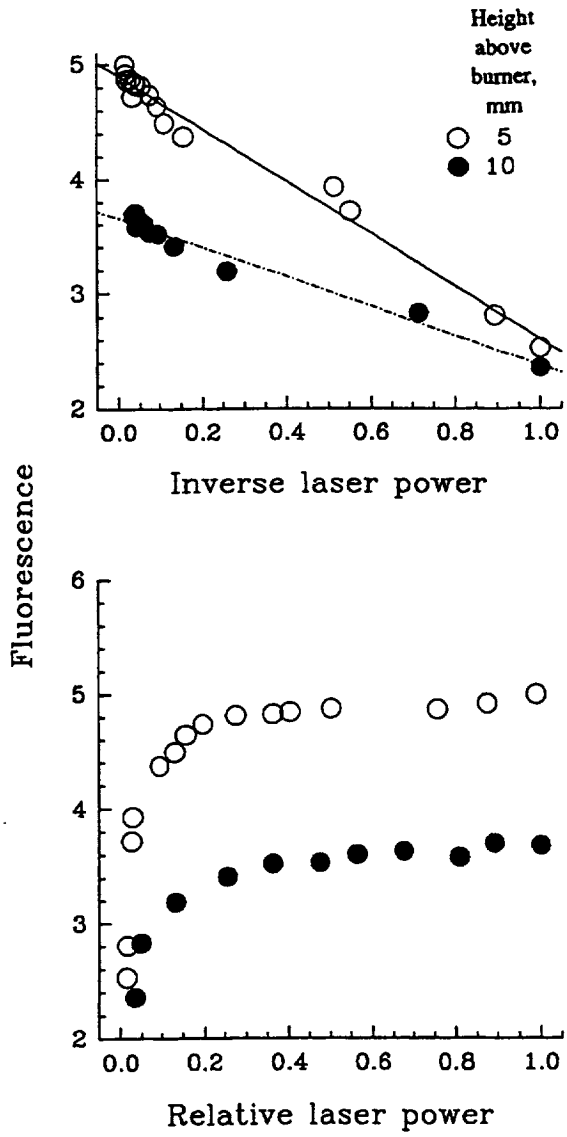

Figure 3.—Saturation curve for flame D. Q_1 (7) excitation; P_1 (8) fluorescence.

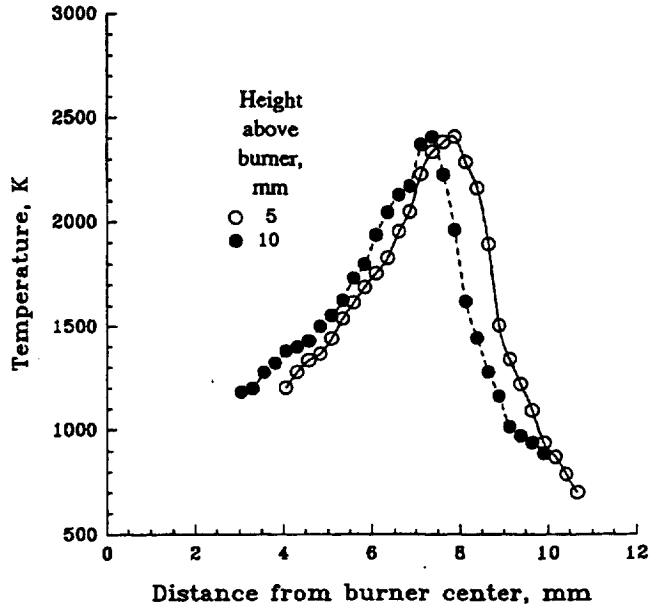

Figure 4.—Temperature distribution profiles measured by two-line LSF method in flame A. The two excited rotational lines are Q_1 (7) and Q_1 (15).

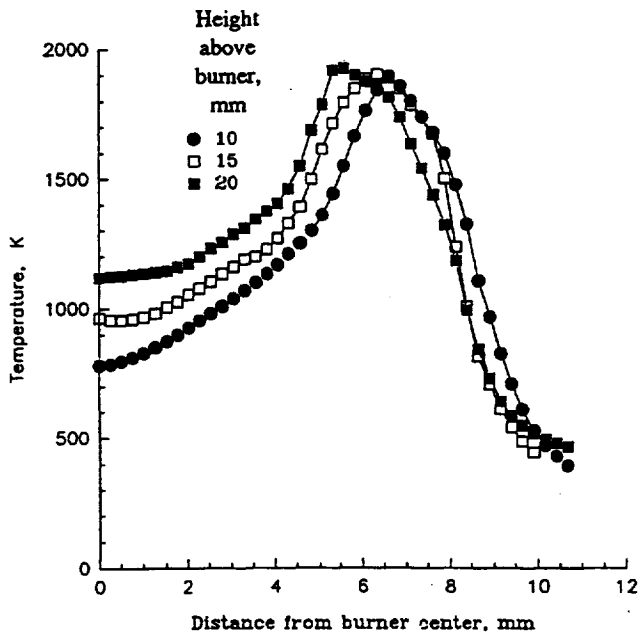

Figure 5.—Temperature distribution profiles measured by 75-μm Pt/Pt-13%Rh thermocouple in flame B.

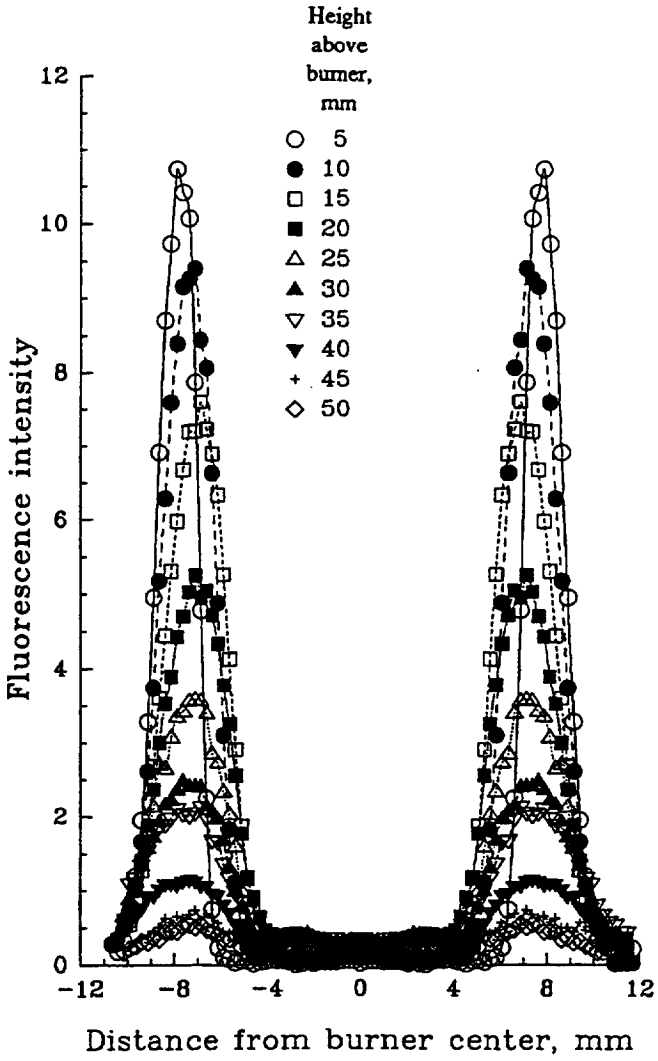

Figure 6.—Relative OH fluorescence profiles for flame A.

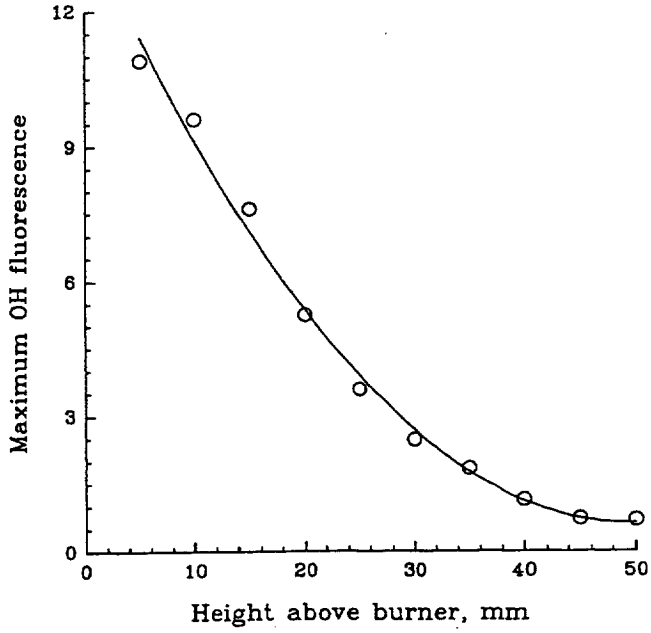

Figure 7.—Local maximum OH fluorescence intensity versus height above burner for flame A.

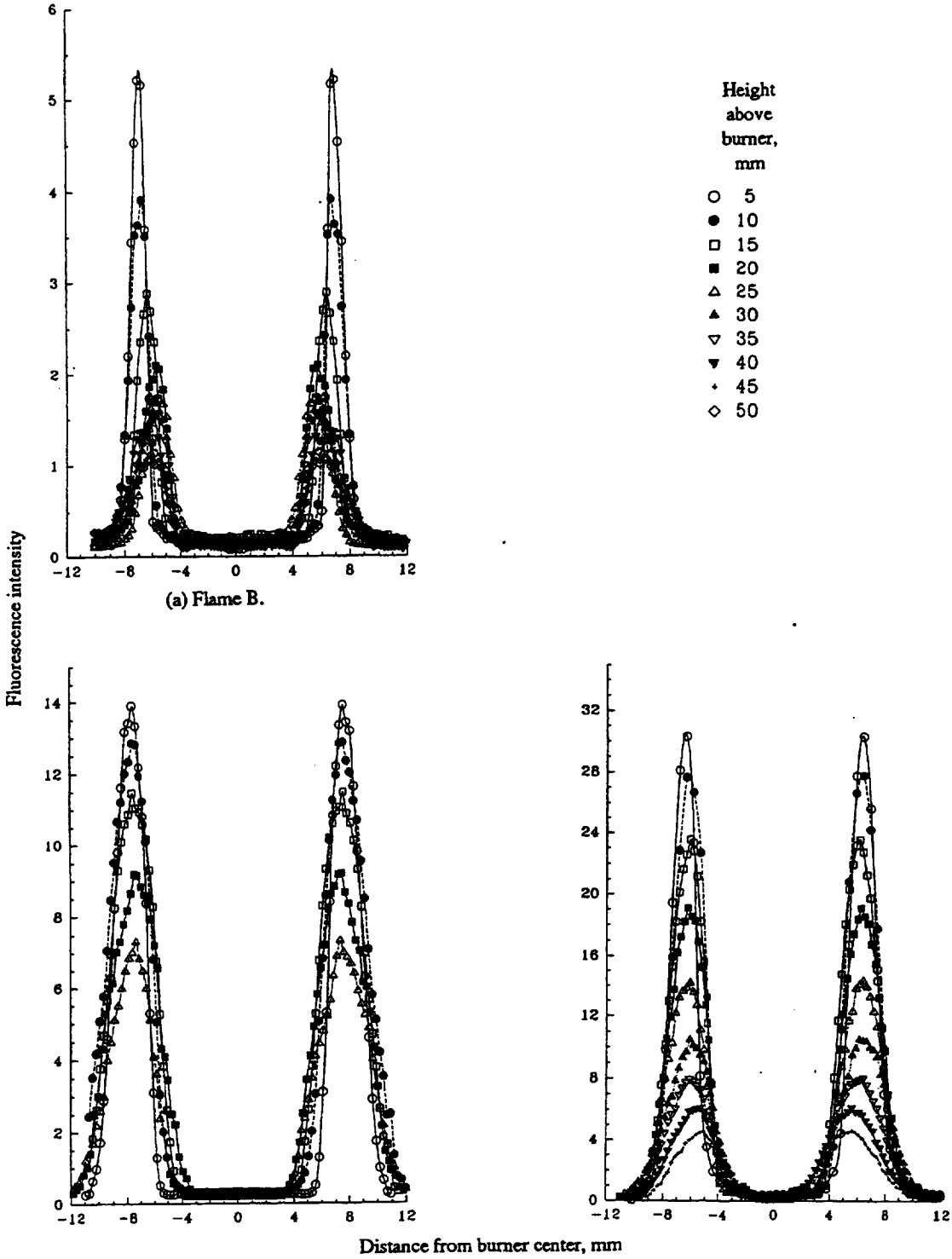

Figure 8.—Relative OH fluorescence profiles for flames B, C, and D.

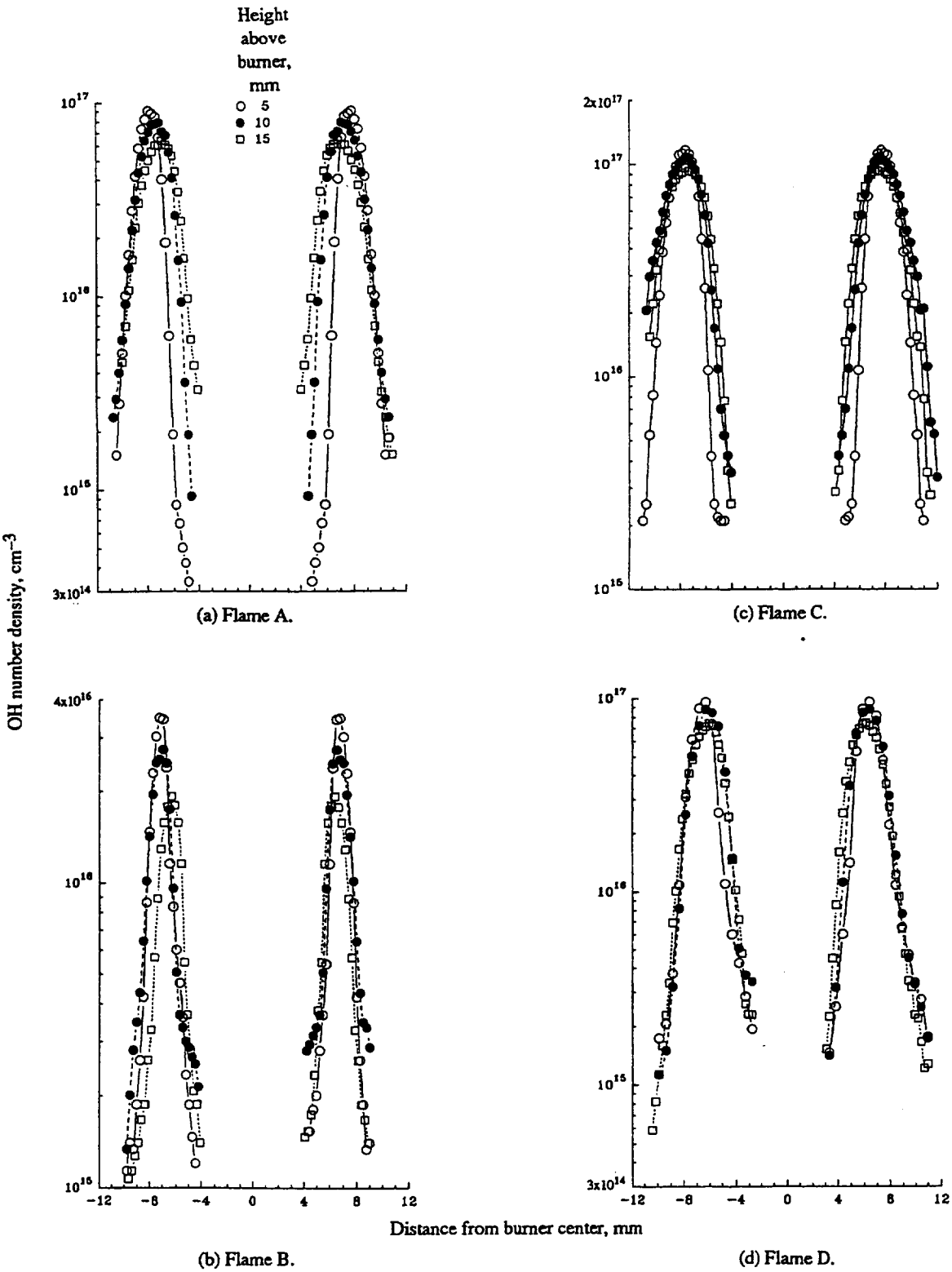

Figure 9.—Hydroxyl concentration profiles for flames A, B, C, and D. Q_1 (7) excitation; P_1 (8) detection.

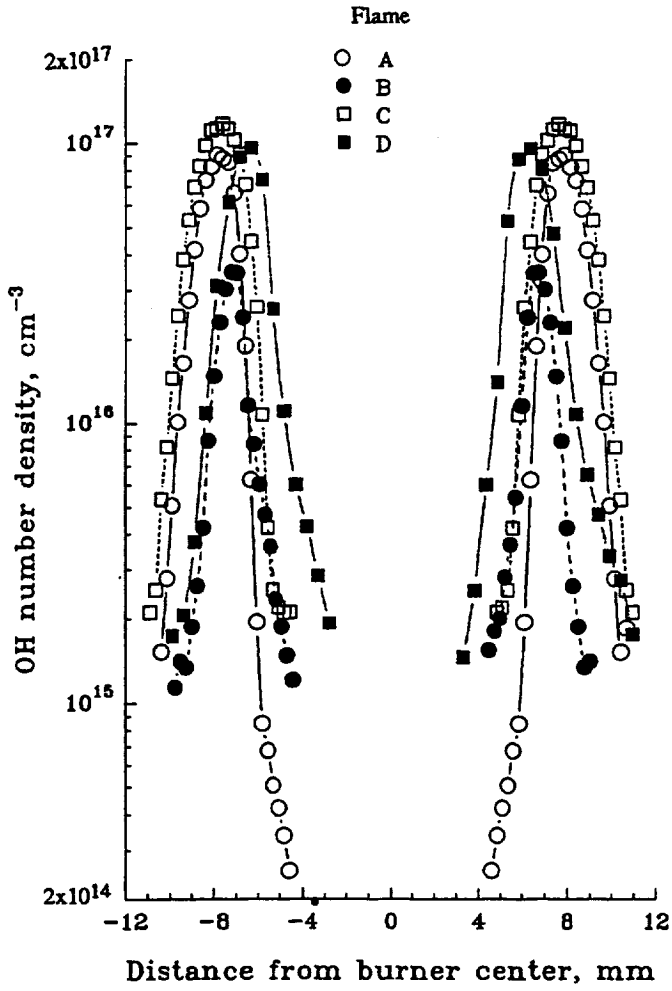

Figure 10.—OH concentration profiles for flames A, B, C, and D measured at 5 mm above burner.

REPORT DOCUMENTATION PAGE

Form Approved
OMB No. 0704-0188

1. AGENCY USE ONLY (*Leave blank*)	2. REPORT DATE	3. REPORT TYPE AND DATES COVERED
	May 1993	Final Contractor Report

4. TITLE AND SUBTITLE

Laser-Saturated Fluorescence Measurements in Laminar Sooting Diffusion Flames

5. FUNDING NUMBERS

WU–505–62–52
C–NAS3–24105

6. AUTHOR(S)

Changlie Wey

7. PERFORMING ORGANIZATION NAME(S) AND ADDRESS(ES)

Sverdrup Technology, Inc.
Lewis Research Center Group
2001 Aerospace Parkway
Brook Park, Ohio 44142

8. PERFORMING ORGANIZATION REPORT NUMBER

E–7771

9. SPONSORING/MONITORING AGENCY NAME(S) AND ADDRESS(ES)

National Aeronautics and Space Administration
Lewis Research Center
Cleveland, Ohio 44135–3191

10. SPONSORING/MONITORING AGENCY REPORT NUMBER

NASA CR–191025

11. SUPPLEMENTARY NOTES

Project Manager, Edward J. Mularz, Internal Fluid Mechanics Division, (216) 433–5850.

12a. DISTRIBUTION/AVAILABILITY STATEMENT

Unclassified - Unlimited
Subject Category 70

12b. DISTRIBUTION CODE

13. ABSTRACT ***(Maximum 200 words)***

The hydroxyl radical is known to be one of the most important intermediate species in the combustion processes. The hydroxyl radical has also been considered a dominant oxidizer of soot particles in flames. In this investigation the hydroxyl concentration profiles in sooting diffusion flames were measured by the laser-saturated fluorescence (LSF) method. The temperature distributions in the flames were measured by the two-line LSF technique and by thermocouple. In the sooting region the OH fluorescence was too weak to make accurate temperature measurements. The hydroxyl fluorescence profiles for all four flames presented herein show that the OH fluorescence intensities peaked near the flame front. The OH fluorescence intensity dropped sharply toward the dark region of the flame and continued declining to the sooting region. The OH fluorescence profiles also indicate that the OH fluorescence decreased with increasing height in the flames for all flames investigated. Varying the oxidizer composition resulted in a corresponding variation in the maximum OH concentration and the flame temperature. Furthermore, it appears that the maximum OH concentration for each flame increased with increasing flame temperature.

14. SUBJECT TERMS

Laser-induced fluorescence; Diffusion flames; Soot; Hydroxyl radical

15. NUMBER OF PAGES

18

16. PRICE CODE

A07

17. SECURITY CLASSIFICATION OF REPORT	18. SECURITY CLASSIFICATION OF THIS PAGE	19. SECURITY CLASSIFICATION OF ABSTRACT	20. LIMITATION OF ABSTRACT
Unclassified	Unclassified	Unclassified	